COMMUNICATION

Check for updates

Origin of the switchable photocurrent direction in BiFeO₃ thin films†

Yaqiong Wang,[abc] Matyas Daboczi, [ID][de] Man Zhang,[b] Joe Briscoe, [ID][b] Ji-Seon Kim, [ID][e] Haixue Yan [ID] *[b] and Steve Dunn*[c]

We report external bias driven switchable photocurrent (anodic and cathodic) in 2.3 eV indirect band gap perovskite (BiFeO₃) photoactive thin films. Depending on the applied bias our BiFeO₃ films exhibit photocurrents more usually found in p- or n-type semiconductor photoelectrodes. In order to understand the anomalous behaviour ambient photoemission spectroscopy and Kelvin-probe techniques have been used to determine the band structure of the BiFeO₃. We found that the Fermi level (E_f) is at −4.96 eV (vs. vacuum) with a mid-gap at −4.93 eV (vs. vacuum). Our photochemically determined flat band potential (E_{fb}) was found to be 0.3 V vs. NHE (−4.8 V vs. vacuum). These band positions indicate that E_f is close to mid-gap, and E_{fb} is close to the equilibrium with the electrolyte enabling either cathodic or anodic band bending. We show an ability to control switching from n- to p-type behaviour through the application of external bias to the BiFeO₃ thin film. This ability to control majority carrier dynamics at low applied bias opens a number of applications in novel optoelectronic switches, logic and energy conversion devices.

New concepts

In this work, we produce a film of BiFeO₃ that demonstrates switchable photocurrents which enable visible light driven anodic and cathodic photochemistry at the functional film and solution interface. Most reports on switchable photocurrent behaviour are associated with production of multi-material systems and it is very rare for simple metal oxide photoelectrodes to show both p- and n-type photocurrent behaviour. By investigating the photochemical and physical properties of the as-obtained BiFeO₃ thin film, we show that it is the band structure and alignment which is responsible for the switchable photocurrents. Our key finding is that BiFeO₃ can be used as a pro-forma system to predict ambipolar behaviour in other materials. This leads to making a contribution to a wide range of applications such as novel optoelectronic switches, optical logic, and energy conversion.

1. Introduction

Switchable photocurrent polarity, such as cathodic to anodic at different applied external bias, is an important subject for the development of advanced optoelectronic systems, logic devices and selective energy conversion approaches.[1–4] This property

[a] *Institute of Medical Engineering, Department of Biophysics, School of Basic Medical Sciences, Health Science Centre, Xi'an Jiaotong University, Xi'an, 710061, China*

[b] *School of Engineering and Materials Science, Queen Mary University of London, Mile End Road, London, E1 4NS, UK. E-mail: h.x.yan@qmul.ac.uk*

[c] *School of Engineering, London South Bank University, 103 Borough Road, London, SE1 0AA, UK. E-mail: dunns4@lsbu.ac.uk*

[d] *Department of Chemical Engineering and Centre for Processable Electronics, Imperial College London, South Kensington, London, SW7 2AZ, UK*

[e] *Department of Physics and Centre for Processable Electronics, Imperial College London, South Kensington, London, SW7 2AZ, UK*

† Electronic supplementary information (ESI) available. See DOI: https://doi.org/10.1039/d3mh01510f

can be found in molecular, hybrid, and inorganic nanoparticle material systems[2,3,5,6] and is quite an unusual phenomenon in single phase metal oxide materials. Demonstrations that molecular photodiodes can switch the direction of a photocurrent under different irradiating light wavelengths[3] give an indication as to the importance of materials that exhibit both p and n type properties. For example, composites of titania nanosheets with polyaniline layers exhibited an n- to p-type switchable photoelectrode behaviour through a range of applied potentials.[5] Similar behaviour was reported in a thin film photoelectrode that consisted of a blend containing n-type Fe₂O₃ and p-type CuFeO₂. In this case the metal oxides were separated into microdomains and demonstrated tunable photo responses under varying applied bias.[2]

To-date, most reports on bipolar photocurrent behaviour are associated with production of multi-material systems. It is very rare for simple metal oxide photoelectrodes to show both p- and n-type photocurrent behaviour. Typical semiconductor photoanodes such those reported in the studies of TiO₂,[7] BiVO₄,[8] Fe₂O₃,[9] *etc.*, or representative photocathodes of Cu-based compounds such as CuBi₂O₄[10] and CuFeO₂[11] act as an electrochemical diode allowing only one direction of current to

flow. Photoelectrochemical (PEC) study has been long used to investigate the photodiode behaviour of a semiconductor. The derived band bending theory well explained the photoanodic behaviour of n-type semiconductor and photocathode behaviour of p-type semiconductor. Normally, no cathodic photocurrents are found in an n-type semiconductor as for a typical n-type semiconductor, the position of Fermi level is close to the conduction band with an energy difference of about $\sim$ 0.1 to 0.2 eV.[12,13] At potentials negative relative to flat band potential there will be excess of majority charge carriers injected to the space charge region. This leads to an accumulation region forming instead of the depletion region. A 'degenerate surface' forms and the semiconductor electrode will behave like a metal electrode with significant carrier transfer in the dark or under illumination and there is no effective photocurrent generated.[12] The inverse but analogous situation occurs in a p-type semiconductor. A very limited number of observations on bipolar photo response from simple metal oxide such as Fe_2O_3[14] and TiO_2[15] have been reported previously. Cathodic photocurrents generation in these photoanode materials was either not explained[14] or attributed to extrinsic contributions such as the co-existence of alkaline electrolyte and the dissolved oxygen in it, which acts as an electron acceptor allowing electron transfer from the photoelectrode surface.[15]

A single-phase semiconductor material exhibiting intrinsic switchable photocurrents is of additional interest compared to conventional semiconductor photoelectrodes, especially in the application of energy conversion, e.g., via the selective PEC oxidation or reduction of water into solar fuels. The realization of practical PEC-based switching devices requires the semiconductor material having suitable band positions, e.g., the conduction band minimum and the valence band maximum straddle the water redox potentials. Meanwhile a material with a narrow band gap which allows visible light absorption is preferable. Other aspects, such as ease of fabrication using earth abundant materials is also important.

$BiFeO_3$ has been extensively studied as it demonstrates room-temperature multiferroic, ferroelectric and magnetic properties and the material is well understood in terms of its physical and chemical properties.[16–18] More recently there has been growing interest in ferroelectric materials as photocatalysts where the spontaneous dipole leads to enhanced carrier separation[19–22] with associated increased chemical reaction rates. $BiFeO_3$ has been extensively studied as it demonstrates room-temperature multiferroic, ferroelectric and magnetic, properties and the material is well understood in terms of its physical and chemical properties.[16–18] More recently there has been growing interest in ferroelectric materials as photocatalysts where the spontaneous dipole leads to enhanced carrier separation[19–22] with associated increased chemical reaction rates. $BiFeO_3$ has been shown to demonstrate an anomalous photovoltage in photovoltaic devices, where the developed photovoltage exceeds the value of the band gap.[23] Strained $BiFeO_3$ films also exhibit a lot of special physical properties such as achieving of abnormal photocurrent through domain wall-defect interaction,[24] short-circuit photocurrent reversing

by the polarization switch[25] and light-induced reversible local ferroelectric polarization.[26] The impact of the inherent electric field of a ferroelectric sample associated with the spontaneous polarization has been demonstrated to influence the photochemical behavior of $BiFeO_3$ in a number of previous studies.[27,28,29] Common to most of these is the poling of a ferroelectric $BiFeO_3$ sample to produce samples with a homogeneous surface domain structure. This previous work has observed that photocurrents changed direction depending on the state of the dipole associated with the poling of the $BiFeO_3$ sample. The photocurrent effectively changed from positive to negative depending on the poling of the surface. This result was attributed to the ferroelectric effect and the generation of a depletion region caused by internal screening within the ferroelectric sample. Such behavior has been observed in a variety of ferroelectric samples where the dipole associated with the polarization of the ferroelectric can drive carrier separation.[22,30]

Herein, we have prepared visible light ($E_g \sim$ 2.3 eV) active ferroelectric $BiFeO_3$ thin film photoelectrodes that exhibit switchable photocurrents around the flat band potential of −4.8 V vs. vacuum through a simple sol–gel method. The $BiFeO_3$ thin film is un-poled with domain polarization direction randomly distributed. Thus ferroelectric effect on the photocurrents direction is limited with a summative compromise among different domains. Origin of the switchable photocurrents has been investigated by PEC methods, well supported by the band structure characterisation results. The specific band structure of the as-prepared $BiFeO_3$ thin film is considered to be the reason of the switchable photocurrents, with a Fermi level that sits near the mid-gap position and both upward and downward band bending allowed under certain applied bias.

2. Results and discussion

Fig. 1a shows the X-ray diffraction (XRD) pattern of the thin film indicating the as-prepared film exhibits high phase purity. The surface morphology of the $BiFeO_3$ electrode, as investigated by scanning electron microscopy (SEM), is shown in Fig. 1b. The micrographs show that the grains range from 50–200 nm in size forming a homogeneous and compact layer on the substrate. The ferroelectric nature of the film was demonstrated by piezo-electric force microscopy (PFM), shown in Fig. S1 (ESI†). The phase image in the PFM indicates that the $BiFeO_3$ film is polycrystalline with different domains randomly oriented with no preferred polarization direction. Ferroelectric switching had been observed using PFM characterization, as shown in Fig. S2 (ESI†), while no switching observed in a further D–E and I–E measurement (Fig. S3, ESI†). The results indicate that the as-prepared $BiFeO_3$ film can be polarized locally, though it is leaking in bulk scale. Our XPS results show that oxygen vacancies existed in the as-prepared $BiFeO_3$ thin films, as well as the co-existence of Fe^{3+} and Fe^{2+} (Fig. S4, ESI†). It is common for $BiFeO_3$ films to have oxygen vacancies and Fe^{2+}, which leading to its leaking nature.[31–33]
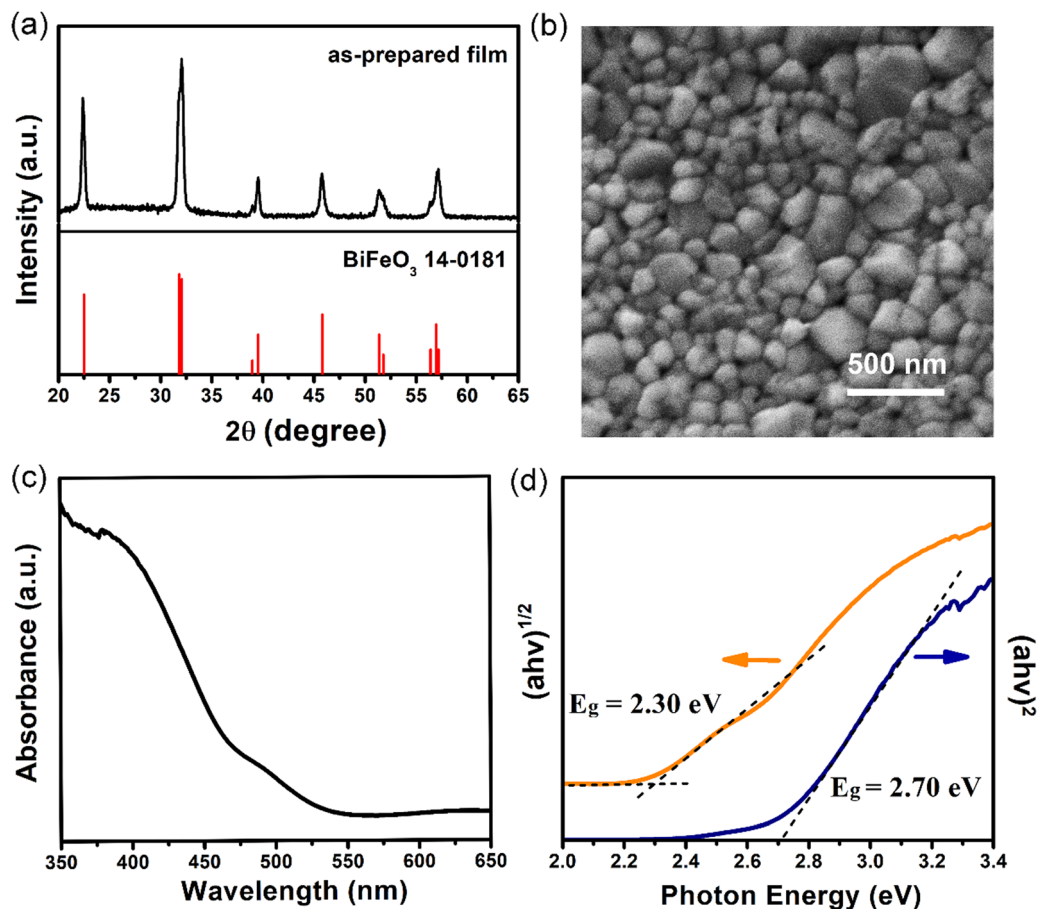
Fig. 1 (a) XRD characterization of the $BiFeO_3$ thin film. (b) SEM image of the $BiFeO_3$ thin film. (c) UV-vis absorption spectrum of the $BiFeO_3$ thin film (d) Derived Tauc plots.

The UV-vis absorption spectrum of the $BiFeO_3$ thin film is shown in Fig. 1c. The absorbance goes through a slow increase from a wavelength of ~ 540 nm followed by a sharp increase around 460 nm. The linear regions in the derived Tauc plots (Fig. 1d) indicate that there are indirect (2.3 eV) and direct band gaps (2.7 eV). $BiFeO_3$ can be viewed as a charge-transfer insulator, with the bandgap controlled by the orbital overlap between the O 2p and the Fe 3d levels.[16] According to previous studies the valence band of $BiFeO_3$ has been considered to be flat.[34] Whereas, the conduction band minimum can vary due to momentum shifts induced by hybridization between the orbital states and the valence state of Fe. This hybridization is dependent on oxygen vacancies and stoichiometry.[34,35] This has led to a wide range of band gaps, from 2.1 eV to 2.8 eV being reported for $BiFeO_3$ thin films. Both indirect/direct band gap characteristics have also been suggested.[34–37] R. Palai et. al have shown that at room temperature (RT) $BiFeO_3$ has an indirect bandgap with a direct gap that lies ~ 0.05 eV above it. In that study the gap becomes more direct with increasing T.[35] The existing body of literature around $BiFeO_3$ indicates that there exist both direct and indirect photoexcitation of electrons at room temperature in $BiFeO_3$. However, the indirect charge transfer mechanism is accepted to dominate at low room temperature.

Our measured values of E_g for both the indirect and direct transition are consistent with current understanding. Therefore, the observed indirect optical bandgap of 2.3 eV will be applied for our discussion regarding the influence of band gap on the photochemical performance of the thin films.

We present current density $vs.$ applied potential plots under chopped simulated solar (AM 1.5) light for $BiFeO_3$ electrode under Na_2SO_4 and Na_2SO_4–H_2O_2 electrolytes in Fig. 2a. H_2O_2 is well known as a good hole scavenger presenting a higher rate constant for oxidation compared to water. It also has a relatively negative reduction potential (E^0 = +0.68 V $vs.$ NHE for the O_2/H_2O_2 couple) $cf.$ water (E^0 = +1.23 V $vs.$ NHE for the O_2/H_2O couple).[38] By increasing the rate of collecting available photo-induced holes at the electrode/electrolyte interface the H_2O_2 containing electrolyte gives a more accurate insight into the on-set potential for photocurrents. This value can be influenced due to the slow carrier transfer kinetics in an aqueous electrolyte solution and causes a shift to be reported. This shift in onset is apparent in our results when the H_2O_2 containing sample is compared against the sample without H_2O_2, Fig. 2a (inset). The on-set potential for both the anodic and cathodic photocurrents can be seen clearly from the plot containing H_2O_2 at around 0.3 V ($vs.$ NHE). The on-set potential of a
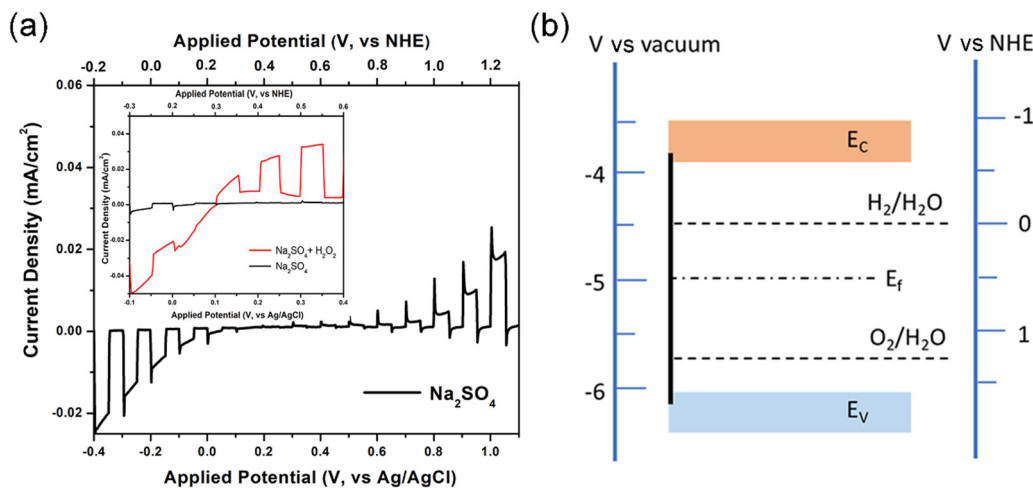
Fig. 2 (a) Current density *vs.* applied potential plots under chopped simulated solar (AM 1.5) light for BiFeO$_3$ electrode under Na$_2$SO$_4$ electrolytes. Inset: Zoom-in of the current density *vs.* applied potential plots in the applied potential range from −0.3 to 0.6 V *vs.* NHE under Na$_2$SO$_4$ and Na$_2$SO$_4$–H$_2$O$_2$ electrolytes. (b) Schematic band diagram of BiFeO$_3$ with respect to the vacuum level and NHE level.

photocurrent is related to the flat band potential of the photo-electrode and indicates the potential at which band bending will start. An accurate electrochemical determination of flat band potential will place it at the same point as the Fermi level determined *via* photophysical techniques.

APS and Kelvin-probe measurements were performed to determine the energy levels of the as-prepared BiFeO$_3$ films. The valence band maximum was measured through photoe-mission procedure. The sample was illuminated with mono-chromatic UV light and the cube root curve of the photoemission obtained and plotted. The valence band maximum (VBM) was determined by APS to be at −6.08 eV, as shown in Fig. S5 (ESI†). Using the indirect band gap value of 2.3 eV, obtained from Tauc analysis, the conduction band minimum was calculated at −3.78 eV. We have measured E_f to be at −4.96 eV (v's vacuum) (shown in Fig. S6, ESI†) and the E_g mid-point at −4.93 eV (v's vacuum). The NHE is regarded to sit at −4.5 eV (v's vacuum) leading to a flat band position of ∼ −4.8 eV (v's vacuum). A schematic band diagram for the BiFeO$_3$ tested is shown in Fig. 2b. The electrochemically measured flat band potential and photo-physcially measured value of E_f are within differences allowable by altered pH at the interface. The conduction band and valence band positions straddle the water redox levels.

It is possible to consider BiFeO$_3$ as a simple semi-conductor if neglects the influence of the ferroelectric nature on the photocurrent produced by BiFeO$_3$. In the thin films presented here each domain exposed to the electrolyte will have an inherent dipole associated with the spontaneous polarization (Fig. S7a and b, ESI†). The interface between the BiFeO$_3$ and electrolyte further influences the band bending due to the movement of carriers across the barrier (Fig. S7c–e, ESI†). When the electrode comes into contact with the electrolyte the bands will align so that E_f at the electrode electrolyte interface is the same as the redox potential of the electrolyte (at 0.615 V v's NHE). In our case this results in an upward band bending of 0.095 eV. This band bending is common across all

domains and is summative. In the case of regions of the BiFeO$_3$ associated with C$^-$ domains the band bending will be increased (Fig. S7c, ESI†). For C$^+$ domains there will be decreased band bending (Fig. S7e, ESI†). For domains with direction parallel to the interface, the spontaneous polarization does not contribute to the interface band bending, only the 0.095 eV upward band bending happens (Fig. S7d, ESI†). In a summary, the C$^+$ domain favors holes transferring out while the C$^-$ domain favors electrons transferring out and they in total give a limited effect on the photocurrents due to the summative compromise among different domains.

The BiFeO$_3$ photoelectrodes investigated here exhibited catho-dic and anodic photocurrents at −ve or +ve applied potentials v's the E_{fb}. This observation is indicative of a material that develops depletion regions associated with p- and n-type semiconductors under the appropriate applied potentials. In our sample we measure the E_f very close to the middle of the band gap (with only 30 meV difference). In a typical n-type semiconductor, the donor concentration dominates and E_f lies close to the conduc-tion band, typically within 0.5 eV.[13] The opposite is found for a p-type semiconductor where the acceptor dominates behavior. In a compensated semiconductor such as BiFeO$_3$ the position of E_f will vary depending on the concentration of the cation vacancy (Bi or Fe vacancy) acting as an acceptor and the oxygen vacancy acting as a donor. BiFeO$_3$ is well known for its complexity arising from the ease of defect formation.[39–43] P-type conductivity is usually observed under normal atmospheric processing conditions with Bi and Fe vacancies dominating, and n-type conductivity is usually observed under oxygen-poor processing conditions with oxygen vacancy dominating.[39,40,44] The BiFeO$_3$ here was prepared by annealing in air and has resulted in E_f and E_g midpoint aligning very closely. This means our samples are self-compensated for defects and exhibit neither strong n- nor p-type characteristics.

The characteristics of band structure, location of E_f and E_g mid-point mean that the BiFeO$_3$ photoelectrode produced here can present both upward and downward band bending at the
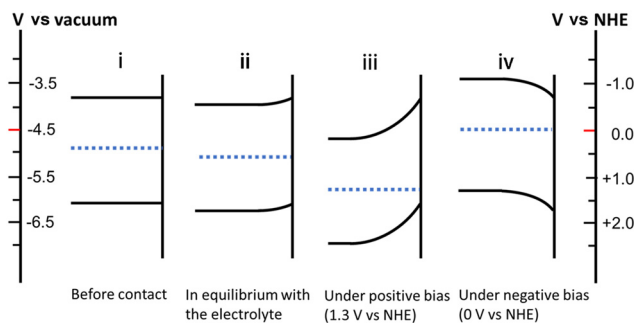
Fig. 3 Schematic band diagrams of (i) a bare $BiFeO_3$ electrode (ii) $BiFeO_3$ electrode in equilibrium with the electrolyte (iii) $BiFeO_3$ electrode under bias positive of the flat band potential (1.3 V *vs.* NHE) (iv) $BiFeO_3$ electrode under bias negative of the flat band potential (0 V *vs.* NHE). Before in contact with the electrolyte solution, there is no charge transfer thus no band bending (i). When the electrode comes into contact with the electrolyte solution, electrons transfer to the electrolyte to achieve equilibrium at which E_f of the electrode is the same as the redox potential of the electrolyte, which is 0.625 V *vs.* NHE. An upward band bending arises followed by the formation of the depletion region (ii). Under potentials positive to that of the flat band potential, E_f shifts more positively and the upward band bending increases (iii), producing anodic photocurrents. A depletion region can also be formed following downward band bending when potentials negative to that of the flat band potential are applied to the electrode, producing cathodic photocurrents.

interface with the electrolyte. Under potentials positive to that of the flat band potential E_f shifts more positively and the upward band bending increases (Fig. 3(iii)). As a result, the depletion region increases and photoexcited charge carriers are separated more efficiently with increased photocurrents being achieved. Under potentials negative to that of the flat potential a depletion region can also be formed following a downward band bending (Fig. 3(iv)). This means that these samples are able to produce both anodic and cathodic currents under the appropriate external bias.

By performing a full investigation of the band structure, in relation not only to the semiconductor but also ferroelectric properties of $BiFeO_3$ photoelectrode films we can explain the observed ambipolar photoresponse of our material. This response comes from a combination of the ferroelectric nature of $BiFeO_3$ and the band structure. However, it seems unlikely that the polar nature of the material has a strong influence on the ambipolar photocurrents. The sample presents randomly oriented domains at the interface between ferroelectric and electrolyte and these findings demonstrate that the ambipolar photocurrents in $BiFeO_3$ photoelectrode are not necessarily controlled by the ferroelectric polarization of the sample. These findings can be used to inform the design of semiconductors with suitable doping levels to achieve a range of tailored photocurrents to meet the requirements of photovoltaic devices and photoelectrochemical cells.

Conclusions

In this study, a switchable photocurrent in $BiFeO_3$ photoelectrode has been studied. The origin of the ambipolar behaviour

has been investigated and explained from the perspective of the energy band levels. The specific bandgap structure of the $BiFeO_3$ photoelectrode provides it with the advantage of generating either anodic or cathodic photocurrents as a function of applied bias. Since the conduction band minimum and valence band maximum of $BiFeO_3$ straddle the water redox potential, it is possible to promote either the hydrogen or the oxygen evolution at one electrode just by tuning the applied potentials and thus allow for selective PEC oxidation or reduction, arousing particular interest for its future application in solar energy conversion. Furthermore, this finding can be adapted to understand and predict other semiconductor photoelectrodes with analogous ambipolar behaviour. It also gives a hint of the way to prepare switchable photoelectrode materials in the future, especially for the compensated semiconductors.

Author contributions

Y. Wang: conceptualization, data curation, formal Analysis, investigation, methodology, validation, visualization, and writing – original draft; M. Daboczi: data curation, formal analysis, methodology, and writing – review & editing; M. Zhang: data curation, formal analysis, and writing – review & editing; J. Briscoe: data curation, formal analysis, and writing – review & editing; J. Kim: data curation, formal analysis, and writing – review & editing; H. Yan: conceptualization, formal analysis, investigation, methodology, supervision and writing – review & editing; S. Dunn: conceptualization, formal analysis, investigation, methodology, funding acquisition, supervision, and writing – review & editing.

Conflicts of interest

The authors declare no conflict of interest.

Acknowledgements

References

1 Y. L. Kim, H. Y. Jung, S. Park, B. Li, F. Liu, J. Hao, Y.-K. Kwon, Y. J. Jung and S. Kar, *Nat. Photonics*, 2014, **8**, 239.
2 R. Beranek and H. Kisch, *Angew. Chem., Int. Ed.*, 2008, **47**, 1320–1322.
3 S. Yasutomi, T. Morita, Y. Imanishi and S. Kimura, *Science*, 2004, **304**, 1944–1947.
4 K. Szaciłowski, W. Macyk and G. Stochel, *J. Am. Chem. Soc.*, 2006, **128**, 4550–4551.
5 B. Seger, J. McCray, A. Mukherji, X. Zong, Z. Xing and L. Wang, *Angew. Chem., Int. Ed.*, 2013, **52**, 6400–6403.
6 A. Efrati, O. Yehezkeli, R. Tel-Vered, D. Michaeli, R. Nechushtai and I. Willner, *ACS Nano*, 2012, **6**, 9258–9266.

7 S. Kment, F. Riboni, S. Pausova, L. Wang, L. Wang, H. Han, Z. Hubicka, J. Krysa, P. Schmuki and R. Zboril, *Chem. Soc. Rev.*, 2017, **46**, 3716–3769.

8 T. W. Kim and K.-S. Choi, *Science*, 2014, **343**, 990–994.

9 B. Iandolo, B. Wickman, I. Zoric and A. Hellman, *J. Mater. Chem. A*, 2015, **3**, 16896–16912.

10 S. P. Berglund, F. F. Abdi, P. Bogdanoff, A. Chemseddine, D. Friedrich and R. van de Krol, *Chem. Mater.*, 2016, **28**, 4231–4242.

11 M. S. Prévot, N. Guijarro and K. Sivula, *ChemSusChem*, 2015, **8**, 1359–1367.

12 S. R. Morrison, *Electrochemistry at semiconductor and oxidized metal electrodes*, Plenum Press, New York and London, 1980.

13 D. A. Neamen, *Semiconductor Physics and Devices: Basic Principles*. 3rd edn, McGraw-Hill, New York, 2003.

14 M. P. Dare-Edwards, J. B. Goodenough, A. Hamnett and P. R. Trevellick, *J. Chem. Soc., Faraday Trans. 1*, 1983, **79**, 2027–2041.

15 A. Tsujiko, H. Itoh, T. Kisumi, A. Shiga, K. Murakoshi and Y. Nakato, *J. Phys. Chem. B*, 2002, **106**, 5878–5885.

16 G. Catalan and J. F. Scott, *Adv. Mater.*, 2009, **21**, 2463–2485.

17 R. K. Vasudevan, Y.-C. Chen, H.-H. Tai, N. Balke, P. Wu, S. Bhattacharya, L. Q. Chen, Y.-H. Chu, I. N. Lin, S. V. Kalinin and V. Nagarajan, *ACS Nano*, 2011, **5**, 879–887.

18 Q. Zhang, D. Sando and V. Nagarajan, *J. Mater. Chem. C*, 2016, **4**, 4092–4124.

19 Y. Cui, J. Briscoe and S. Dunn, *Chem. Mater.*, 2013, **25**, 4215–4223.

20 M. R. Morris, S. R. Pendlebury, J. Hong, S. Dunn and J. R. Durrant, *Adv. Mater.*, 2016, **28**, 7123–7128.

21 Y. Wang, M. Zhang, J. Liu, H. Zhang, F. Li, C.-W. Tseng, B. Yang, G. Smith, J. Zhai, Z. Zhang, S. Dunn and H. Yan, *Adv. Energy Mater.*, 2020, **10**, 2001802.

22 Y. Liu, S. Ye, H. Xie, J. Zhu, Q. Shi, N. Ta, R. Chen, Y. Gao, H. An, W. Nie, H. Jing, F. Fan and C. Li, *Adv. Mater.*, 2020, **32**, 1906513.

23 T. Choi, S. Lee, Y. J. Choi, V. Kiryukhin and S.-W. Cheong, *Science*, 2009, **324**, 63–66.

24 H.-B. Zhang, M.-M. Yang and M. Alexe, *Adv. Photonics Res.*, 2023, **4**, 2200189.

25 Y. Yang, W. Xu, X. Xu, Y. Wang, G. Yuan, Y. Wang and Z.-G. Liu, *J. Appl. Phys.*, 2016, **119**, 044102.

26 M.-M. Yang and M. Alexe, *Adv. Mater.*, 2018, **30**, 1704908.

27 Q. Liu, Y. Zhou, L. You, J. Wang, M. Shen and L. Fang, *Appl. Phys. Lett.*, 2016, **108**, 022902.

28 D. Cao, Z. Wang, N. Nasori, L. Wen, Y. Mi and Y. Lei, *Angew. Chem.*, 2014, **126**, 11207–11211.

29 J. H. Shah, H. Ye, Y. Liu, A. M. Idris, A. S. Malik, Y. Zhang, H. Han and C. Li, *J. Mater. Chem. A*, 2020, **8**, 6863–6873.

30 G. Wan, L. Yin, X. Chen, X. Xu, J. Huang, C. Zhen, H. Zhu, B. Huang, W. Hu, Z. Ren, H. Tian, L. Wang, G. Liu and H. M. Cheng, *J. Am. Chem. Soc.*, 2022, **144**, 20342–20350.

31 Y. Shuai, S. Zhou, S. Streit, H. Reuther, D. Bürger, S. Slesazeck, T. Mikolajick, M. Helm and H. Schmidt, *Appl. Phys. Lett.*, 2011, **98**, 232901.

32 Z. Zhang, P. Wu, L. Chen and J. L. Wang, *Appl. Phys. Lett.*, 2010, 96.

33 M. Makarovic, N. Kanas, A. Zorko, K. Ziberna, H. Ursic, D. R. Smabraten, S. M. Selbach and T. Rojac, *J. Eur. Ceram. Soc.*, 2020, **40**, 5483–5493.

34 S. J. Clark and J. Robertson, *Appl. Phys. Lett.*, 2007, **90**, 132903.

35 R. Palai, R. Katiyar, H. Schmid, P. Tissot, S. Clark, J. Robertson, S. Redfern, G. Catalan and J. Scott, *Phys. Rev. B: Condens. Matter Mater. Phys.*, 2008, **77**, 014110.

36 J. Ihlefeld, N. Podraza, Z. Liu, R. Rai, X. Xu, T. Heeg, Y. Chen, J. Li, R. Collins and J. Musfeldt, *Appl. Phys. Lett.*, 2008, **92**, 142908.

37 Y. Xu and M. Shen, *Mater. Lett.*, 2008, **62**, 3600–3602.

38 H. Dotan, K. Sivula, M. Gratzel, A. Rothschild and S. C. Warren, *Energy Environ. Sci.*, 2011, **4**, 958–964.

39 Q. Xu, M. Sobhan, Q. Yang, F. Anariba, K. P. Ong and P. Wu, *Dalton Trans.*, 2014, **43**, 10787–10793.

40 T. R. Paudel, S. S. Jaswal and E. Y. Tsymbal, *Phys. Rev. B: Condens. Matter Mater. Phys.*, 2012, **85**, 104409.

41 M. Schrade, N. Masó, A. Perejón, L. A. Pérez-Maqueda and A. R. West, *J. Mater. Chem. C*, 2017, **5**, 10077–10086.

42 S. Clark and J. Robertson, *Appl. Phys. Lett.*, 2009, **94**, 022902.

43 X. Qi, J. Dho, R. Tomov, M. G. Blamire and J. L. MacManus-Driscoll, *Appl. Phys. Lett.*, 2005, **86**, 062903.

44 Z. Zhang, P. Wu, L. Chen and J. Wang, *Appl. Phys. Lett.*, 2010, **96**, 232906.